

Ultraprecision Machining Characteristics of Poly-Crystalline Germanium*

Jiawang YAN**, Yasunori TAKAHASHI***, Jun'ichi TAMAKI***,
Akihiko KUBO***, Tsunemoto KURIYAGAWA** and Yutaka SATO****

Germanium is an excellent infrared optical material. On most occasions, single-crystalline germanium is used as optical lens substrate because its homogeneous structure is beneficial for fabricating uniform optical surfaces. In this work, we attempt to use poly crystals as lens substrates instead of single crystals, which may lead to a significant reduction in production cost. We conducted ultraprecision cutting experiments on poly-crystalline germanium to examine the microscopic machinability. The crystal orientations of specific crystal grains were characterized, and the machining characteristics of these crystal grains including surface textures, cutting forces, and grain boundary steps were investigated under various machining conditions. It was possible to produce uniformly ductile-cut surfaces cross all crystal grains by using an extremely small undeformed chip thickness (~ 80 nm) under negative tool rake angles ($\sim -45^\circ$). This work indicates the possibility of fabricating high-quality infrared optical components from poly-crystalline germanium.

Key Words: Ultraprecision Machining, Diamond Turning, Ductile Regime Machining, Poly Crystal, Germanium, Optical Surface

1. Introduction

Germanium (Ge) is an excellent infrared optical material which has high permeability and high refractive index in the infrared wavelength range. It is a major substrate material for infrared optical components with extensive applications in thermal imaging systems, dark-field optical instruments, infrared astronomical telescopes, and so on. According to the microstructure, germanium can be divided into poly crystals and single crystals. On most occasions, single-crystalline germanium (*s*-Ge) is currently used as optical substrate, because its homogeneous structure is beneficial for fabricating uniform optical surfaces. However, due to the technical difficulties in growing large-diameter *s*-Ge ingots, the production cost of large-diameter optical lenses is very high.

In this work, we attempt to use poly-crystalline germanium (*p*-Ge) as optical-lens substrates to substitute *s*-Ge. This innovation, if succeeds, will lead to a significant reduction in production costs for infrared optical components. However, germanium is a highly brittle material with strong crystallographic anisotropy. Thus, the microscopic mechanical properties vary with crystal grains, resulting in significantly different processing behaviors. This anisotropic effect will cause nonuniformity in surface quality and eventually limit the productivity of the manufacturing processes.

Among various optical manufacturing technologies, single-point diamond turning (SPDT) has been demonstrated to be capable of machining complex geometries with nanometer level accuracy. Previous studies have found that *s*-Ge undergoes high-pressure phase transformations which gives rise to plastic deformation during indentation, scratching and machining tests^{(1)–(5)}. The feasibility for fabricating infrared Fresnel lenses from *s*-Ge by SPDT has also been demonstrated by some of the present authors⁽⁶⁾. On the other hand, to date, little literature can be found on the ultraprecision machining of *p*-Ge. In this work, we conducted ultraprecision cutting experiments on *p*-Ge to examine its microscopic machinability. The crystal orientations of specific crystal grains were character-

* Received 31st October, 2005 (No. 05-4233)

** Department of Nanomechanics, Tohoku University, 6–6–01 Aoba, Aramaki, Aoba-ku, Sendai 980–8579, Japan.
E-mail: yanjw@pm.mech.tohoku.ac.jp

*** Department of Mechanical Engineering, Kitami Institute of Technology, 165 Koen-cho, Kitami, Hokkaido 090–8507, Japan

**** Department of Material Processing, Tohoku University, 6–6–02 Aoba, Aramaki, Aoba-ku, Sendai 980–8579, Japan

ized and their machining characteristics were investigated. The critical conditions for producing uniform smooth surfaces on all crystal grains were experimentally examined.

2. Materials and Methods

2.1 Machining apparatus

Machining experiments were carried out on an ultra-precision lathe TOYODA AHP 20–25 N. A schematic illustration of the lathe is shown in Fig. 1 (a). It has a hydrostatic bearing spindle and two perpendicular slide tables along the X-axis and the Z-axis. The slide table driving system has a two-level structure: a hydraulic system for coarse motion and a servomotor system for fine motion. A precision tool post is installed on the Z-axis table. This tool post can rotate in the X-Z plane and enables fine adjustment of the cutting edge angle of cutting tools. Four air mounts were set under the machine base to isolate environmental vibrations. A tool holder equipped with a three-component piezoelectric dynamometer (Kistler 9251A) was used to measure cutting forces. The cutting force signal processing system is schematically shown in Fig. 1 (b). In order to achieve an exact correspondence between the

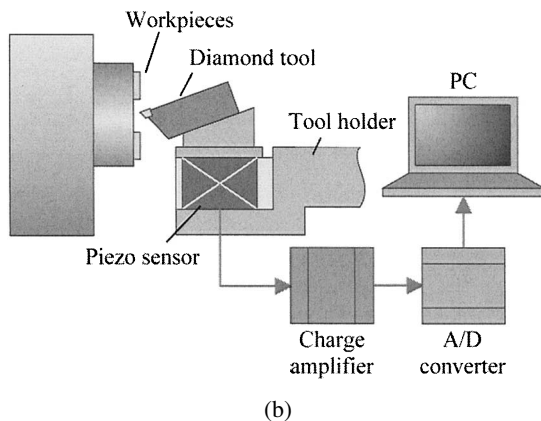
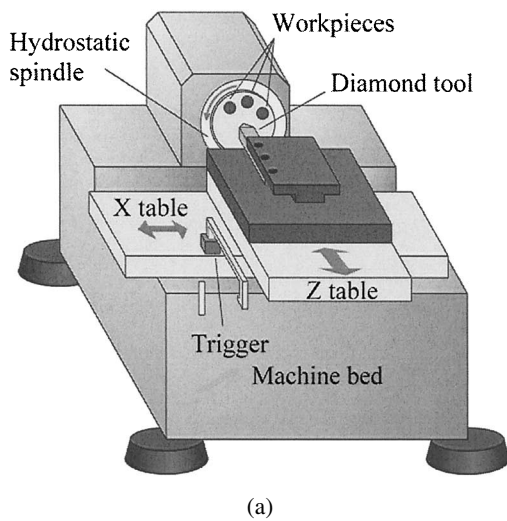


Fig. 1 Schematic illustrations of (a) ultra-precision lathe and (b) cutting force measurement setup

cutting force signals and the cutting positions during multiple cuts, a positioning trigger was set onto the X-axis table to indicate the starting point of measurement.

2.2 Machining model

Straight-nosed cutting tools⁽⁷⁾ made of single-crystal diamond were used for machining. The machining model is schematically shown in Fig. 2. The tool moves longitudinally with periodical transverse feeds, hence regular shallow grooves are generated on the workpiece surface. For this tool geometry, undeformed chip thickness (h) is uniform across the entire width of the cutting edge. Thus, the relationship between the surface texture and the undeformed chip thickness is unambiguous and readily studied. The relationship among undeformed chip thickness h , cutting edge angle κ and tool feed f can be described by Eq. (1):

$$h = f \cdot \sin \kappa \quad (1)$$

Thus, by varying cutting edge angle κ and/or tool feed f , it is possible to change the undeformed chip thickness h from the micron level to the nanometer level.

2.3 Machining conditions

A diamond tool which has a nominal rake angle of 0° and a nominal relief angle of 6° was used. The tool rake face was tilted with tapered steel blocks to obtain negative rake angles down to -45° . It must be supplemented that due to the inclination of the tool, the relief angle was also changed, from 6° to 51° . Here, to use negative rake angles was to achieve a compressive stress field ahead the cutting edge, which is essential for ductile machining of hard brittle materials⁽⁸⁾.

Three pieces of p -Ge substrates were used as workpieces. The workpieces are 10 mm in diameter, 3 mm in thickness and obtained with polished finishes. In order to characterize the distributions and orientations of crystal grains, an orientation-imaging microscopic (OIM) system produced by TexSEM Laboratories, Inc. was used. Figure 3 shows the grain map and the pole figures of three

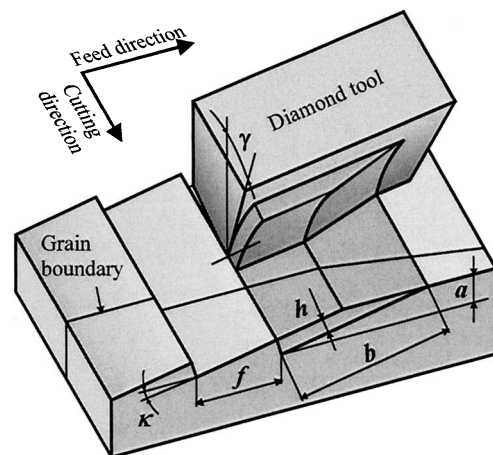


Fig. 2 Machining model

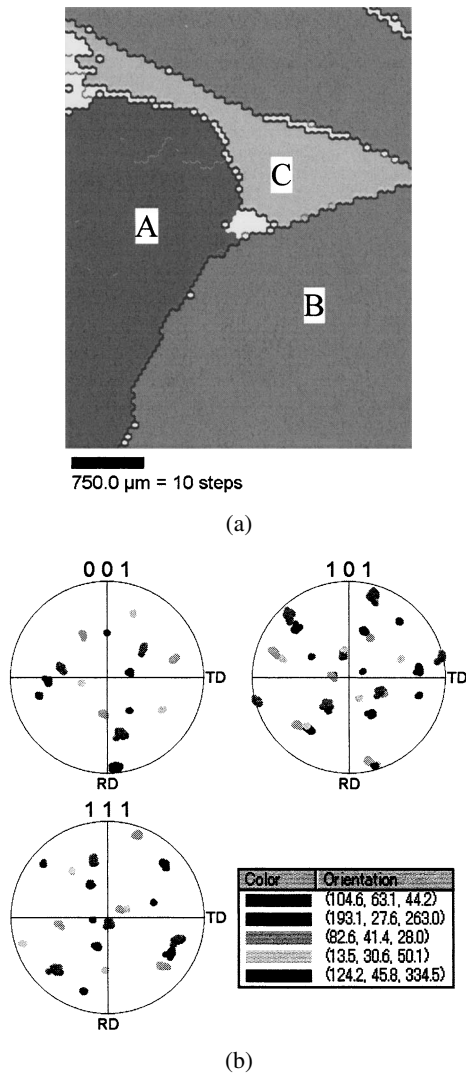


Fig. 3 OIM analysis results: (a) grain map, and (b) pole figures showing orientations of each grain

crystal grains indicated by A, B and C, which were selected to be investigated emphatically in this work. The sizes of these grains were relatively large, thus it is easy for surface characterization. From the OIM results, the boundaries and the crystalline orientations of the crystal grains can be clearly identified. The workpieces were bonded to a diamond-turned aluminum blank (diameter 125 mm) using a heat-softened glue and then vacuum-chucked to the machine spindle.

Machining conditions used in the experiments are summarized in Table 1. Depth of cut a was set to $2\ \mu\text{m}$. Undeformed chip thickness h was varied from a few nanometers to 700 nm, by changing tool feed f in the range of $7\text{--}37.5\ \mu\text{m}$ and cutting edge angle κ in the range of $0.15\text{--}1.45^\circ$. The rotation rate of the machine spindle was fixed to 800 rpm, consequently, the cutting speed changes in the range of $4.8\text{--}5.2\ \text{m/s}$. Dry cuts were performed without coolant. A Nomarski differential interference microscope, a scanning electron microscope (SEM),

Table 1 Machining conditions

Machining method	Face turning
Workpiece	Poly-crystalline germanium
Cutting tool	Single-crystal diamond tool
Rake angle γ	$0^\circ, -20^\circ, -45^\circ$
Relief angle α	$6^\circ, 26^\circ, 51^\circ$
Spindle rotation rate	800 rpm
Depth of cut a	$2\ \mu\text{m}$
Feed rate f	$7\text{--}37.5\ \mu\text{m/rev}$
Cutting edge angle κ	$0.15\text{--}1.45^\circ$

a laser-probe scanning three-dimensional measuring machine, and an atomic force microscope (AFM) were used to examine and measure the machined surfaces. The cutting chips were also observed using the SEM.

3. Results and Discussion

3.1 Surface textures

Figure 4 is a Nomarski differential interference micrograph of the machined surface near the grain boundaries of crystal grains A, B and C shown in Fig. 3. Apparently, the surface textures of these grains are very different, some are very smooth and the others are damaged by micro pits. Therefore, grain boundaries can be identified clearly among these grains. Figure 5 is the magnified micrographs of these crystal grains. The parallel bright lines seen on the surfaces are the tool marks corresponding to the periodical tool feeds. In Fig. 5 (a), the surface is severely damaged with numerous micro craters and cracks, the size of which ranges from 1 to $10\ \mu\text{m}$ level. In Fig. 5 (b), the surface is extremely smooth, without any micro-fractures. In Fig. 5 (c), the surface is generally smooth, but dotted with a few micro-fractures in $1\ \mu\text{m}$ order.

Germanium has a strong directional covalent bond with the diamond-cubic structure. The cleavage plane is $\{111\}$ and the predominant slip system is $\{111\} [110]$. During machining $p\text{-Ge}$, the orientations of the cleavage planes and slip systems changes as the tool passes different crystal grains. Consequently, the cleavage/slipping behavior will be location-dependent, and it determines whether brittle fracture or plastic deformation occurs. An analytical model of the crystallographic effect on machining behavior using a phase-transformation model and the Schmid's factor will be further discussed elsewhere in another coming paper.

3.2 Chip morphologies

Figure 6 is SEM micrographs of the chips obtained at various undeformed chip thicknesses. These chips are removed from multiple crystal grains, thus it is difficult to identify the relationship between the chip morphology

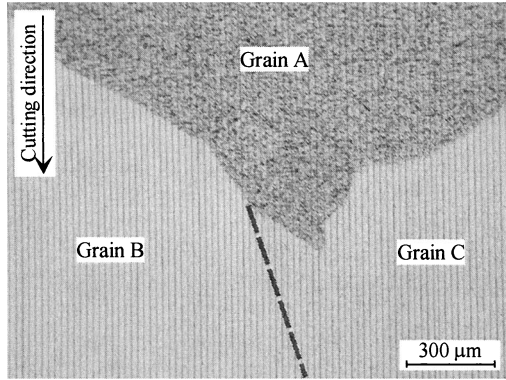
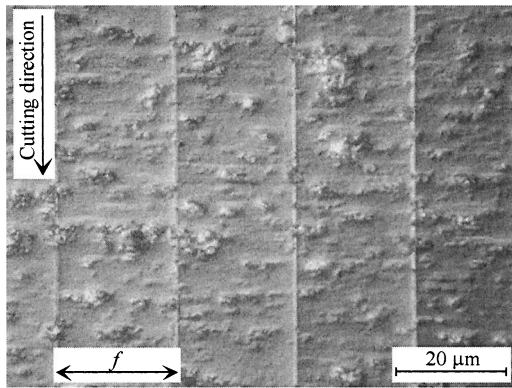
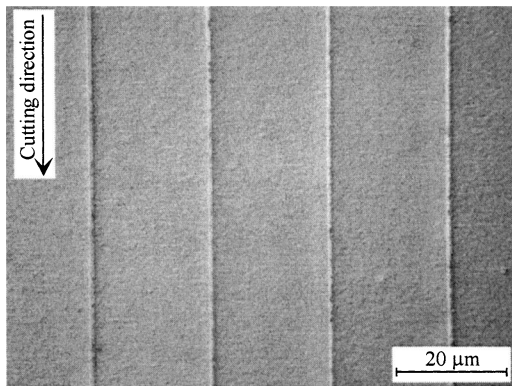


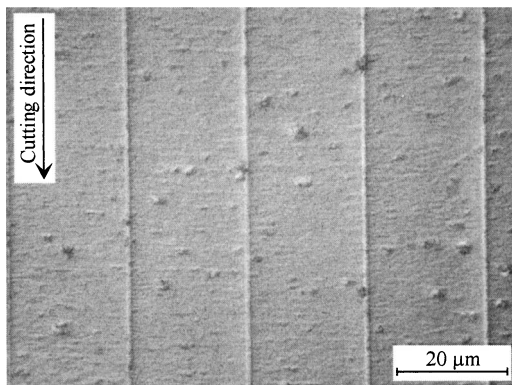
Fig. 4 Nomarski micrograph of machined surface near grain boundaries at conditions $\gamma = -20^\circ$ and $h = 318$ nm



(a)

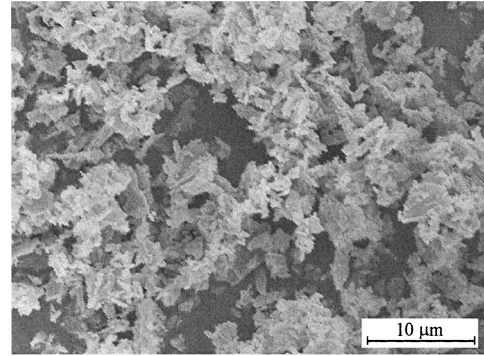


(b)

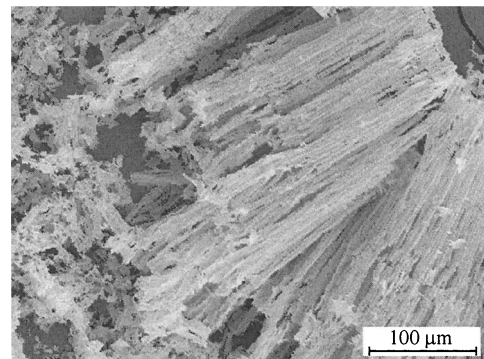


(c)

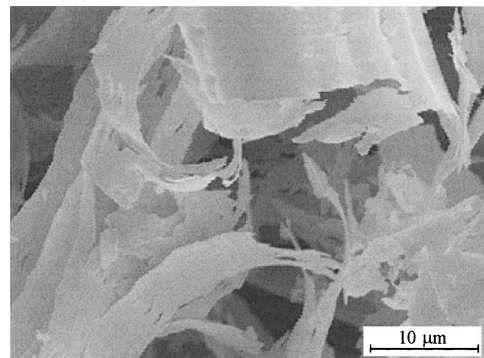
Fig. 5 Magnified photographs of the crystal grains shown in Fig. 4: (a) grain A, (b) grain B and (c) grain C



(a)



(b)



(c)

Fig. 6 SEM photographs of chips obtained at various undeformed chip thicknesses: (a) 639 nm, (b) 269 nm, and (c) 65 nm, using a -45° rake angle tool

and the crystal orientation. However, the overall trend of chip formation behavior with respect to undeformed chip thicknesses is clear. In Fig. 6 (a), the chips are micro particles and blocks, irregular in shape, with fractured appearance. These chips indicate that brittle fracture has been predominant during material removal. In Fig. 6 (b), the chips consist of both fine particles and regular needles with similar shapes, indicating a brittle-ductile transition mode. In Fig. 6 (c), the chips are in the form of curled ribbons similar to those of ductile metal cutting, indicating that plastic deformation has been occurring dominantly in this machining regime.

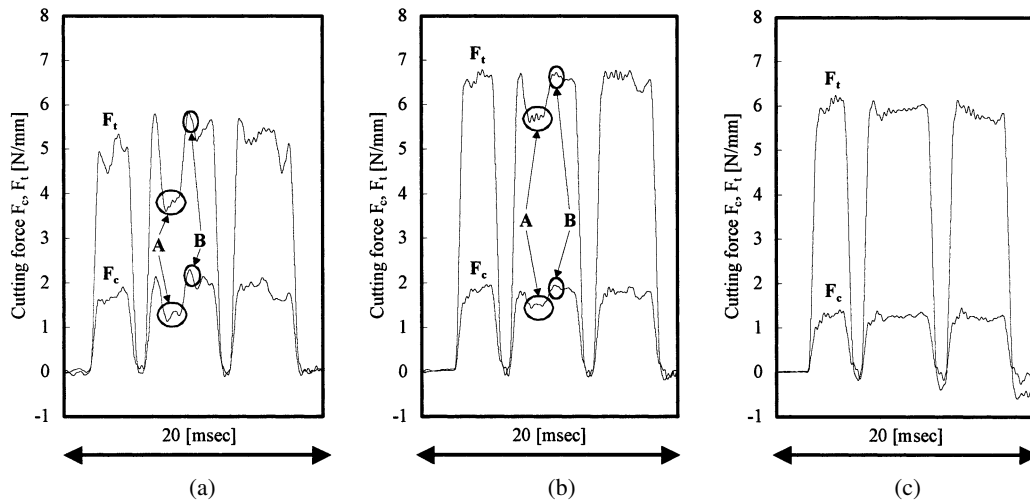


Fig. 7 Principal and thrust cutting force wavinesses measured when machining at various undeformed chip thicknesses: (a) 693 nm, (b) 131 nm, and (c) 42 nm, using a -20° rake angle tool

3.3 Micro cutting forces

Figure 7 shows the wavinesses of principal cutting force F_c and thrust cutting force F_t acting on per mm-width of cutting edge during cutting at different undeformed chip thicknesses. At a big undeformed chip thickness (Fig. 7(a)) where all the crystal grains were cut in the brittle regimes, both F_c and F_t depend on crystal grains and the force signals fluctuated significantly. Those grains which have been severely damaged by brittle fractures correspond to smaller forces, and those slightly damaged correspond to larger forces. However, this crystal-grain dependence of cutting forces becomes insignificant as undeformed chip thickness decreases, as shown in Fig. 7(b). When undeformed chip thickness is decreased to 42 nm (Fig. 7(c)), where all crystal grains are ductile-machined, the force variation becomes very small and is not noticeable.

3.4 Grain boundary step

The surface regions near the grain boundaries were measured to characterize the grain boundary steps. Figure 8(a) is a Nomarski micrograph of the surface near the boundary between two adjoining crystal grains, A and B, which were machined at an undeformed chip thickness of 56 nm using a -45° rake angle tool. Although both of the grains have been machined in a ductile mode, a slight dark line can be seen in the middle of the photograph, indicating the existence of a grain boundary step. Figure 8(b) is an AFM image of a small region near the grain boundary. In the figure, the saw-toothed surface profile generated by periodical tool feed demonstrates a perfect transcription between the cutting edge and the work-piece. Across the tool feed marks, a grain boundary step can be clearly identified, which corresponds to the dark line shown in Fig. 8(a). Figure 8(c) is a cross-sectional profile of the boundary which is measured along the cut-

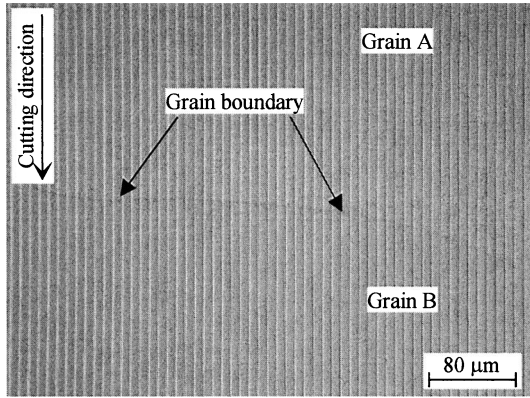
ting direction. The grain boundary step is approximately 20 nm high.

The formation mechanism of grain boundary steps during machining poly-crystalline materials is a complex problem, and is still an area of controversy. A grain boundary may result from multiple effects of material anisotropy, tool geometry, and the rigidity of machining systems. Supposing that the machine rigidity is sufficiently high, the predominant factor for grain boundary step will be material anisotropy. An orthogonal machining model is shown in Fig. 9. Beneath and ahead of the cutting tool, the material will be subjected to severe plastic and elastic deformation. However, after the tool has passed, the elastic deformation will recover and causes a rise in surface height. Because the elastic modulus depends on crystal orientations, boundary steps will then be generated after the strain has been released to different degrees. From this point of view, it may be said that to eliminate boundary steps, it is essential to enhance the plastic deformation and at the same time to prevent from significant elastic deformation.

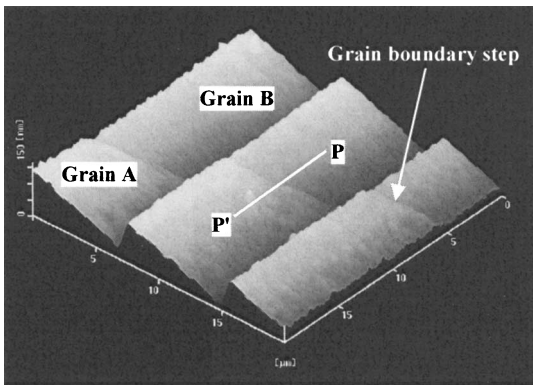
Figure 10 shows the relationship between undeformed chip thickness and the heights of crystal grain boundary steps. As undeformed chip thickness increases, the boundary step height also increases. This result is due to the fact that smaller undeformed chip thicknesses cause more plastic deformation and less elastic deformation in brittle materials. From this result, we can also say that an extremely small undeformed chip thickness is essential for producing smooth optical surfaces without noticeable boundary steps.

3.5 Effects of tool rake angles

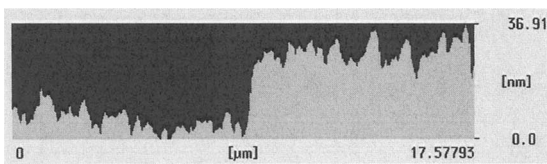
Tool rake angle has been known to be a key process parameter for ductile regime machining of brittle materials. Negative rake angle can produce compressive stress



(a)



(b)



(c)

Fig. 8 (a) Nomarski micrograph, (b) AFM image, and (c) cross-sectional profile of a grain boundary step. Machining conditions are $h = 56 \text{ nm}$, $\gamma = -45^\circ$. The profile in (c) is measured from P to P' indicated in (b)

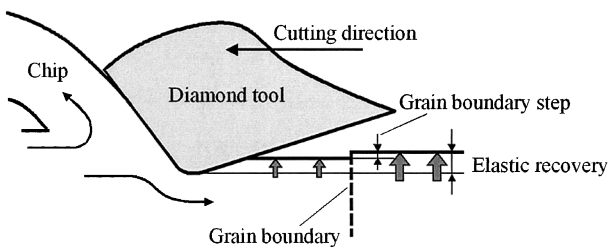


Fig. 9 Schematic model of grain boundary step formation mechanism

field involving hydrostatic pressure which is beneficial for ductile-regime material removal⁽⁸⁾⁻⁽¹¹⁾. In this work, tool rake angle was changed from 0 to -45° to examine its effects on the machining characteristics of *p*-Ge.

Figure 11 shows the variations in surface roughness

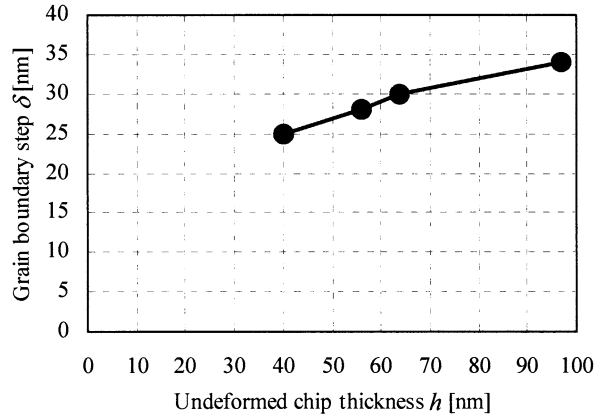
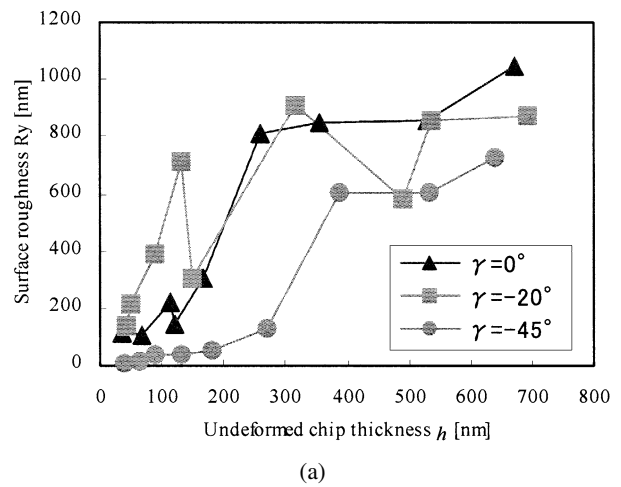
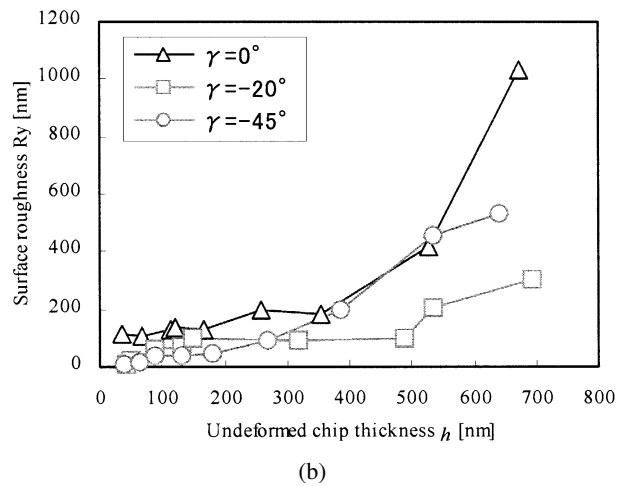


Fig. 10 Relationship between undeformed chip thickness and the heights of crystal grain boundary steps



(a)



(b)

Fig. 11 Variations in surface roughness of crystal grains A and B machined with different rake angle tools at various undeformed chip thicknesses

of crystal grains A and B machined with different rake angle tools at various undeformed chip thicknesses. The surface roughness was measured along the cutting direction and the influence of the tool feed marks was not considered; thus the surface roughness can exactly represent the

orthogonal cutting behavior. From the figure, it is clearly seen that for both crystal grains, higher negative rake angle tools produce lower surface roughness, and generally the -45° rake angle tool works the best. The advantage of high negative rake angle might be due to the burnishing effect which has been confirmed in metal machining. Under the present conditions, by using an extremely small undeformed chip thickness (~ 80 nm) under the -45° rake angle tool, uniform ductile-cut surfaces with the nanometer level roughness were obtained on all the examined crystal grains.

4. Summary

In order to explore the feasibility of using polycrystalline germanium as infrared optical lens substrates instead of single crystals, we conducted ultraprecision cutting experiments on polycrystalline germanium to examine its microscopic machinability. The machining characteristics of various crystal grains including machined surface textures, cutting forces, and grain boundary steps were investigated under various machining conditions. Uniformly ductile-cut surfaces were obtained cross all crystal grains by using an extremely small undeformed chip thickness (~ 80 nm) under high negative tool rake angles (-45°). The possibility of fabricating high-quality infrared optical components using polycrystalline germanium has been demonstrated.

Acknowledgements

This work has been partially supported by the industrial technology research grant program (04A31508) from the Japan New Energy and Industrial Technology Development Organization (NEDO).

References

- (1) Clarke, D.R., Kroll, M.C., Kirchner, P.D. and Cook, R.F., Amorphization and Conductivity of Silicon and Germanium Induced by Indentation, *Phys. Rev. Lett.*, Vol.60, No.21 (1988), pp.2156–2159.
- (2) Morris, J.C., Callahan, D.L., Kulik, J., Patten, J.A. and Scattergood, R.O., Origins of the Ductile Regime in Single-Point Diamond Turning of Semiconductors, *J. Am. Ceram. Soc.*, Vol.78, No.8 (1995), pp.2015–2020.
- (3) Nakasuji, T., Kodera, S., Hara, S., Matsunaga, H., Ikawa, N. and Shimada, S., Diamond Turning of Brittle Materials for Optical Components, *Ann. CIRP*, Vol.39, No.1 (1990), pp.89–92.
- (4) Blake, P.N. and Scattergood, R.O., Ductile Regime Machining of Germanium and Silicon, *J. Am. Ceram. Soc.*, Vol.73, No.4 (1990), pp.949–957.
- (5) Yan, J., Maekawa, K., Tamaki, J. and Kubo, A., Experimental Study on the Ultraprecision Ductile Machinability of Single-Crystal Germanium, *JSME Int. J., Ser. C*, Vol.47, No.1 (2004), pp.29–36.
- (6) Yan, J., Maekawa, K., Tamaki, J. and Kuriyagawa, T., Micro Grooving on Single-Crystal Germanium for Infrared Fresnel Lenses, *J. Micromech. Microeng.*, Vol.15 (2005), pp.1925–1931.
- (7) Yan, J., Syoji, K., Kuriyagawa, T. and Suzuki, H., Ductile Regime Turning at Large Tool Feed, *J. Mater. Proc. Tech.*, Vol.121 (2002), pp.363–372.
- (8) Yan, J., Syoji, K. and Kuriyagawa, T., Ductile-Brittle Transition under Large Negative Rake Angles, *J. Jpn. Soc. Prec. Eng.*, (in Japanese), Vol.66, No.7 (2000), pp.1130–1134.
- (9) Bridgman, P.W., The Effect of Hydrostatic Pressure on the Fracture of Brittle Substances, *J. Appl. Phys.*, Vol.18 (1947), pp.246–258.
- (10) Yan, J., Syoji, K. and Kuriyagawa, T., Some Aspects on the Optimization of Ductile Regime Cutting Process, *Proc. Inter. Conf. on Adv. Manuf. Sys. & Manuf. Auto.*, Guangzhou, China, June 19–21, (2000), pp.185–189.
- (11) Yan, J., Yoshino, M., Kuriyagawa, T., Shirakashi, T., Syoji, K. and Komanduri, R., On the Ductile Machining of Silicon for Micro Electro-Mechanical Systems (MEMS), *Opto-Electronic and Optical Applications, Mater. Sci. Eng., A*, Vol.297, No.1–2 (2001), pp.230–234.